RESEARCH ARTICLE

Transdifferentiation as a Mechanism of Treatment Resistance in a Mouse Model of Castration-Resistant Prostate Cancer

Min Zou[1], Roxanne Toivanen[2], Antonina Mitrofanova[3], Nicolas Floch[4], Sheida Hayati[5], Yanping Sun[6], Clémentine Le Magnen[1], Daniel Chester[4], Elahe A. Mostaghel[7], Andrea Califano[8], Mark A. Rubin[9], Michael M. Shen[10], and Cory Abate-Shen[11]

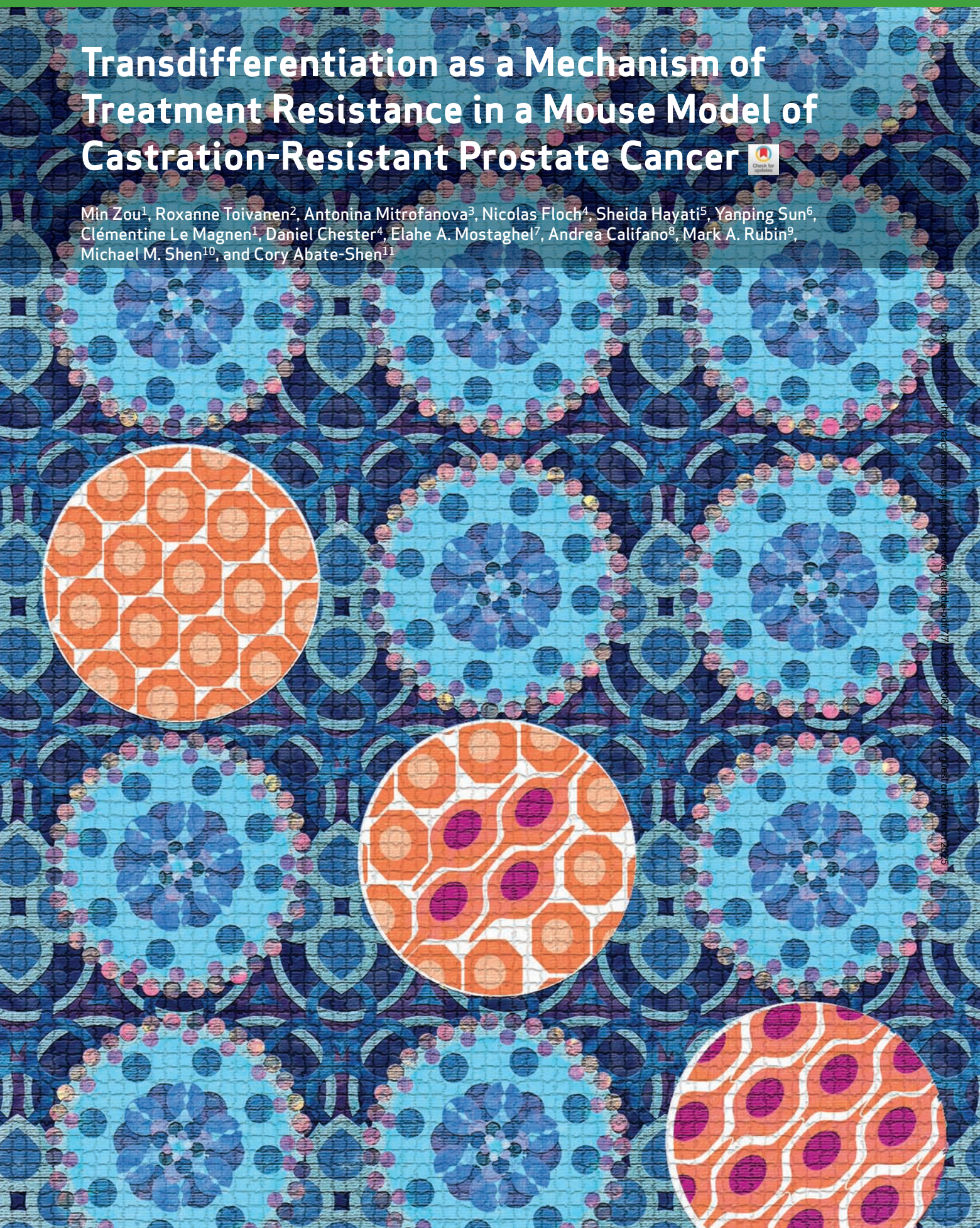

ABSTRACT Current treatments for castration-resistant prostate cancer (CRPC) that target androgen receptor (AR) signaling improve patient survival, yet ultimately fail. Here, we provide novel insights into treatment response for the antiandrogen abiraterone by analyses of a genetically engineered mouse (GEM) model with combined inactivation of *Trp53* and *Pten*, which are frequently comutated in human CRPC. These NPp53 mice fail to respond to abiraterone and display accelerated progression to tumors resembling treatment-related CRPC with neuroendocrine differentiation (CRPC-NE) in humans. Cross-species computational analyses identify master regulators of adverse response that are conserved with human CRPC-NE, including the neural differentiation factor *SOX11*, which promotes neuroendocrine differentiation in cells derived from NPp53 tumors. Furthermore, abiraterone-treated NPp53 prostate tumors contain regions of focal and/or overt neuroendocrine differentiation, distinguished by their proliferative potential. Notably, lineage tracing *in vivo* provides definitive and quantitative evidence that focal and overt neuroendocrine regions arise by transdifferentiation of luminal adenocarcinoma cells. These findings underscore principal roles for *TP53* and *PTEN* inactivation in abiraterone resistance and progression from adenocarcinoma to CRPC-NE by transdifferentiation.

SIGNIFICANCE: Understanding adverse treatment response and identifying patients likely to fail treatment represent fundamental clinical challenges. By integrating analyses of GEM models and human clinical data, we provide direct genetic evidence for transdifferentiation as a mechanism of drug resistance as well as for stratifying patients for treatment with antiandrogens. *Cancer Discov; 7(7); 736–49. ©2017 AACR.*

See related commentary by Sinha and Nelson, p. 673.

INTRODUCTION

Prostate adenocarcinoma, one of the most common cancers affecting aging men, is characterized by its profoundly different outcomes depending on disease stage. Although locally invasive prostate cancer generally has a favorable prognosis, progression to metastatic disease results in high mortality as current treatment modalities are not yet curative, despite significant progress in recent years (1, 2). For many decades, androgen-deprivation therapy (ADT) has been a mainstay for treatment of advanced or recurrent prostate adenocarcinoma, due to the requirement of androgen receptor (AR) signaling at all stages of disease progression (3, 4). ADT initially results in tumor regression, but ultimately leads to relapse with a more aggressive and often metastatic disease, termed castration-resistant prostate cancer (CRPC, sometimes referred to as CRPC-Adeno), which retains an adenocarcinoma phenotype and remains dependent on AR signaling despite depletion of androgens (3, 4). Treatments for CRPC have focused on inhibition of AR or androgen biosynthesis using antiandrogen agents such as enzalutamide or abiraterone (1). Although these agents improve survival, these gains are often transient, as most patients ultimately fail treatment (1, 4). Notably, treatment failure is often associated

[1]Departments of Medicine and Urology, Institute of Cancer Genetics, Herbert Irving Comprehensive Cancer Center, Columbia University Medical Center, New York, New York. [2]Departments of Medicine and Genetics and Developmental Biology, Institute of Cancer Genetics, Herbert Irving Comprehensive Cancer Center, Columbia University Medical Center, New York, New York. [3]Department of Systems Biology, Columbia University Medical Center, New York, New York; and Department of Health Informatics, Rutgers, The State University of New Jersey, Newark, New Jersey. [4]Department of Urology, Columbia University Medical Center, New York, New York. [5]Department of Health Informatics, Rutgers, The State University of New Jersey, Newark, New Jersey. [6]Department of Medicine, Columbia University Medical Center, New York, New York. [7]Clinical Research Division, Fred Hutchinson Cancer Research Center, Seattle, Washington. [8]Departments of Systems Biology, Biomedical Informatics, and Biochemistry and Molecular Biophysics, Center for Computational Biology and Bioinformatics, Institute of Cancer Genetics, Herbert Irving Comprehensive Cancer Center, Columbia University Medical Center, New York, New York. [9]Englander Institute for Precision Medicine and Department of Pathology and Laboratory Medicine, Weil Cornell Medical College and New York-Presbyterian Hospital, New York, New York. [10]Departments of Medicine, Genetics and Development, Urology, and Systems Biology, Institute of Cancer Genetics, Herbert Irving Comprehensive Cancer Center, Columbia University Medical Center, New York, New York. [11]Departments of Urology, Medicine, Systems Biology, and Pathology and Cell Biology, Institute of Cancer Genetics, Herbert Irving Comprehensive Cancer Center, Columbia University Medical Center, New York, New York.

Note: Supplementary data for this article are available at Cancer Discovery Online (http://cancerdiscovery.aacrjournals.org/).

M. Zou and R. Toivanen contributed equally to this article.

Current address for A. Mitrofanova: Department of Health Informatics, Rutgers, The State University of New Jersey, Newark, NJ; current address for N. Floch: Oncology iMED, AstraZeneca, Cambridge, UK; and current address for D. Chester: Louisiana State University, Health Sciences Center, New Orleans, LA.

Corresponding Authors: Cory Abate-Shen, Columbia University Medical Center, 1130 St. Nicholas Avenue, New York, NY 10032. Phone: 212-851-4731; Fax: 212-851-4787; E-mail: cabateshen@columbia.edu; and Michael Shen, Columbia University Medical Center, 1130 St. Nicholas Avenue, New York, NY 10032. Phone: 212-851-4723; Fax: 212-851-4572; E-mail: mshen@columbia.edu

doi: 10.1158/2159-8290.CD-16-1174

with the emergence of a highly aggressive variant, which has histopathologic features of small-cell carcinoma and neuroendocrine (NE) differentiation, often mixed together with adenocarcinoma, termed CRPC-NE (5–8). Notably, although small-cell/neuroendocrine-like histopathology is extremely rare in localized prostate cancer (9, 10), emerging clinical data suggest that a substantial proportion of patients that fail ADT develop CRPC-NE (7, 8, 11).

Correlating with their distinct disease outcomes, genomic sequencing analyses have revealed that locally invasive and advanced prostate cancer have profound differences in their mutational landscapes (12–18). In particular, primary prostate tumors have a paucity of single-nucleotide variants and instead feature copy-number alterations such as deletion of 8p21, resulting in haploinsufficiency for the *NKX3.1* homeobox gene, and genomic rearrangements such as *TMPRSS2–ERG* (13, 16, 18). In contrast, CRPC and metastatic disease display frequent oncogenic driver mutations, including in the *TP53* and *PTEN* tumor suppressor genes, which are often comutated (15, 17).

Here, we have investigated the consequences of coinactivation of *TP53* and *PTEN* for treatment response to the antiandrogen abiraterone using a genetically engineered mouse (GEM) model of CRPC. Strikingly, we show that abiraterone treatment of these NPp53 mice often results in tumor progression to a small-cell/neuroendocrine-like phenotype. Notably, we show by lineage tracing that these neuroendocrine-like cells arise by transdifferentiation of luminal prostate adenocarcinoma cells, underscoring the significance of lineage plasticity as a mechanism of drug resistance.

RESULTS

A Refined GEM Model of CRPC Is Conserved with Human CRPC

The most common somatic alterations in human CRPC are predicted to result in loss of function of *TP53* and *PTEN*. In particular, whole-exome sequencing of biopsies from men with metastatic CRPC as reported by the Stand Up To Cancer (SU2C) consortium revealed that alterations of *TP53*, including missense mutations, deletions, and truncations, occurred in 50% of cases ($n = 150$ patients), whereas those affecting *PTEN*, which were mostly deletions, occurred in 40% of cases ($n = 150$; Fig. 1A and B; Supplementary Table S1; ref. 17). Similarly, whole-exome sequencing of metastatic CRPC tumors obtained at autopsy also have frequent somatic alterations of *TP53* and *PTEN* (54% for *TP53* and 50% for *PTEN*, $n = 48$ patients; ref. 15). Notably, the prevalence of *TP53* alterations in CRPC contrasts with their infrequent occurrence in locally invasive primary tumors (<10%, $n = 333$ patients; Fig. 1B; refs. 14, 16, 18). Furthermore, although comutation of *TP53* and *PTEN* is rare in primary tumors (<2%), such comutations are highly prevalent in metastatic CRPC from biopsies (23% co-occurrence, $n = 150$; $P < 0.0001$; Fisher exact test; Fig. 1B; ref. 17) and tumors (33%, $n = 48$; $P < 0.0001$; Fisher exact test; ref. 15).

Given the prevalence of their coinactivation in human CRPC, we sought to investigate the consequences of combined loss of function of *Pten* and *Trp53* for treatment of CRPC using a GEM model based on an inducible *Nkx3.1*^{CreERT2} driver to delete these genes in adult prostate epithelium (19). Our approach has distinct advantages over previous GEM models of *Pten* and *Trp53* loss of function in prostate, which used a constitutive Cre driver that is mostly specific to prostate, but is not restricted to adults or a specific epithelial cell type (20, 21). In contrast, the *Nkx3.1*^{CreERT2} driver is a knock-in allele in which a tamoxifen-inducible CreERT2 cassette is placed under the transcriptional control of the endogenous *Nkx3.1* promoter, resulting in heterozygous inactivation of *Nkx3.1* and thereby resulting in preinvasive phenotypes (19). Induction of Cre activity by tamoxifen administration enables temporal control of gene deletion in mature adult prostate, as well as spatial restriction to prostatic luminal epithelial cells (19, 22), which are a cell of origin for prostate cancer (23), and enables lineage tracing to define the cellular origin of tumor phenotypes.

Because GEM models with loss of function of *Trp53* alone have modest prostate cancer phenotypes (20, 24, 25), whereas those with loss of function of *Pten* alone develop prostate adenocarcinoma and CRPC (21, 26), we compared the phenotype of *Trp53* and *Pten* compound mutant mice with that of *Pten* single-mutant mice. In particular, we analyzed the prostate phenotype of two different inducible GEM models, corresponding to *Nkx3.1*$^{CreERT2/+}$; *Pten*$^{flox/flox}$; *Trp53*$^{flox/flox}$ mice (NPp53 mice) and *Nkx3.1*$^{CreERT2/+}$; *Pten*$^{flox/flox}$ mice (NP mice, previously described, ref. 26) under normal androgen conditions (hormonally intact mice) or following androgen ablation by surgical castration (Fig. 1C; Supplementary Table S2). As expected, castration resulted in profound reduction of testosterone (T) and dihydrotestosterone (DHT) in both NP and NPp53 mice to barely detectable levels (Supplementary Fig. S1A). Furthermore, following castration, both the NP and NPp53 mice develop CRPC that retains features of adenocarcinoma (Fig. 1C; Supplementary Table S2), thereby resembling human CRPC-Adeno, similar to previously reported GEM models based on loss of function of *Pten* and *Trp53* (20, 21). Notably, the CRPC phenotype in the NP and NPp53 mice shows appropriate expression of epithelial cytokeratins, consistent with the luminal phenotype of prostate adenocarcinoma, and has a high proliferative index (Fig. 1C; Supplementary Table S2). As expected, AR displays primarily nuclear localization in prostate tumor cells of hormonally intact mice, but is more diffusely localized in *NP* and *NPp53* CRPC (Fig. 1C).

To extrapolate preclinical studies from these GEM models to human CRPC, we sought to establish whether the molecular pathways that drive CRPC in NP and NPp53 mice are conserved with those that drive CRPC in humans. Toward this end, we used the Master Regulator Inference algorithm (MARINa) to identify master regulators (MR) that drive CRPC in these GEM models, and then performed cross-species computational analyses to evaluate their conservation with MRs that drive human CRPC (see detailed experimental methods in Supplementary Materials, and ref. 27). For this purpose, we generated mouse MR signatures representing the transition to CRPC in the NP or NPp53 mice (NP CRPC vs. N and NPp53 CRPC vs. N, respectively, with N representing the control *Nkx3.1*^{CreERT2} mice), or comparing the CRPC in NPp53 and NP mice (NPp53 CRPC vs. NP CRPC). We then performed cross-species gene set enrichment analysis (GSEA) by querying these mouse MR signatures with several independent human MR signatures that are indicative of specific biological phenotypes of prostate cancer and/or CRPC-Adeno (Supplementary Table S1).

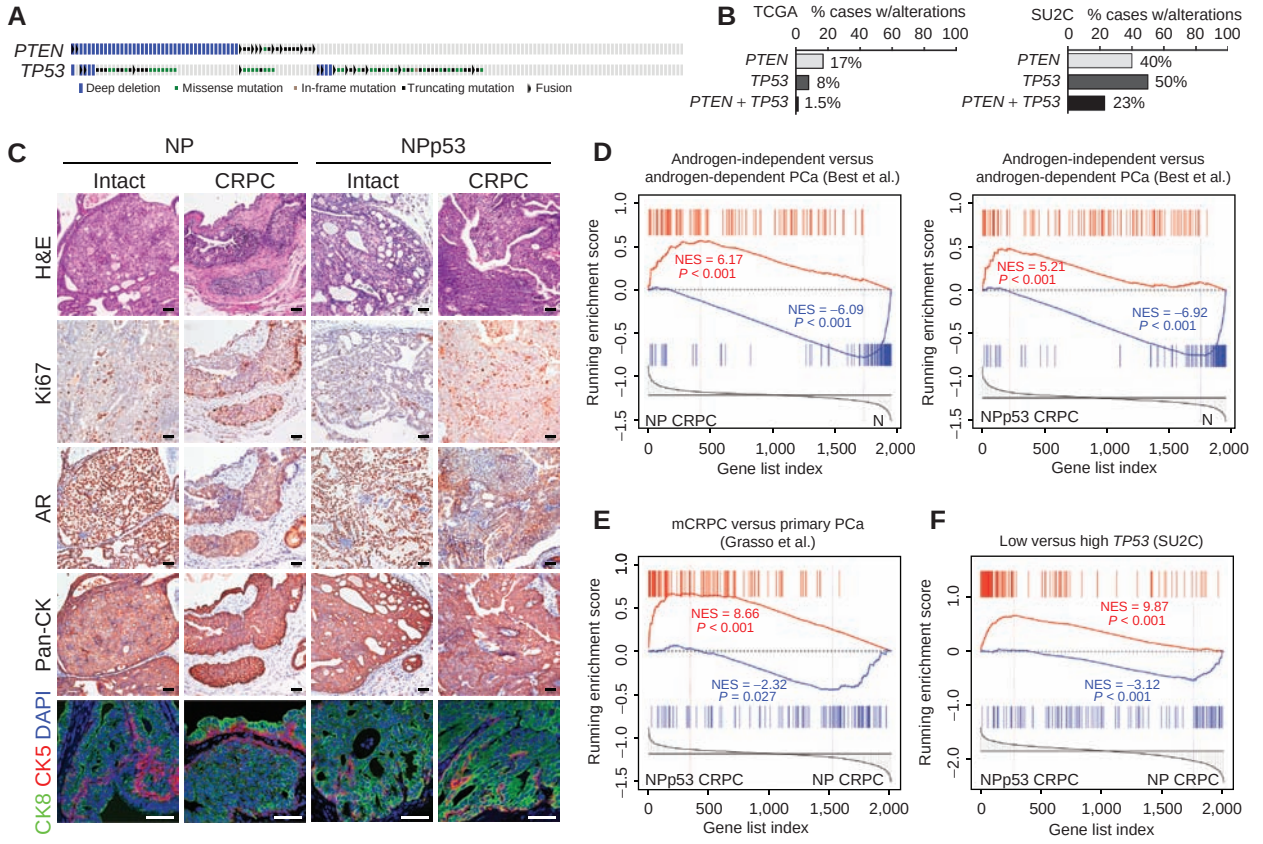

Figure 1. A refined GEM model of CRPC is conserved with human CRPC. **A** and **B,** *PTEN* and *TP53* gene alterations in human prostate cancer. **A,** Oncoprint depicting alterations of *PTEN* and *TP53* in metastatic CRPC as reported by the SU2C consortium. **B,** Prevalence of alterations in primary prostate tumors [from The Cancer Genome Atlas (TCGA); ref. 16] and metastatic CRPC (from SU2C; ref. 17). **C,** Phenotypic analyses of GEM models. Histopathologic analyses of androgen-intact prostate tumors or CRPC from NP and NPp53 mice, as indicated. Shown are representative hematoxylin and eosin (H&E) images and representative immunostaining for the indicated antibodies. Scale bars, 50 μm. **D–F,** Cross-species GSEAs. **D,** Comparison of reference mouse MR signatures from NP CRPC (left) or NPp53 CRPC (right) versus control mouse prostate (N) with a query human MR signature compares treatment-naïve androgen-independent versus androgen-dependent primary prostate tumors (PCa; $n = 10$/group) from Best et al. (28). **E,** Comparison of reference mouse MR signature from NPp53 CRPC versus NP CRPC with a query human MR signature comparing metastatic CRPC ($n = 35$) versus primary tumors (PCa; $n = 59$) from Grasso et al. (15). **F,** Comparison of reference mouse MR signature from NPp53 CRPC versus NP CRPC with a query human MR signature comparing metastatic CRPC having low *PTEN*/low *TP53* versus low *PTEN*/high *TP53* ($n = 5$/group from SU2C). In **D–F**, "NES" stands for normalized enrichment score; GSEA *P* values were calculated using 1,000 gene permutations. See also additional related analyses in Supplementary Fig. S1 and Supplementary Table S1 for description of human datasets, and Supplementary Dataset 1 for complete list of differentially expressed genes in the mouse tumors.

First, we asked whether molecular drivers associated with the transition to CRPC in these GEM models are conserved with those in humans by querying the relevant mouse MR signatures (NP CRPC vs. N and NPp53 CRPC vs. N) with a human MR signature of treatment-naïve androgen-independent primary tumors ($n = 10$) versus androgen-dependent tumors ($n = 10$) from Best and colleagues (ref. 28; Supplementary Table S1). Cross-species GSEA revealed a striking enrichment of MR signatures for both mouse models ($P < 0.001$; Fig. 1D), indicating a strong conservation of the molecular drivers of CRPC between the mouse and human tumors.

Next, we asked whether CRPC in NPp53 versus NP mice is representative of more advanced, metastatic CRPC in humans, as might be anticipated given the additional *Trp53* loss of function. For this, we compared a mouse MR signature of NPp53 CRPC versus NP CRPC with a human MR signature from metastatic CRPC ($n = 35$) versus localized prostate cancer ($n = 59$) from Grasso and colleagues (ref. 15; Supplementary Table S1). Cross-species GSEA revealed a strong enrichment particularly of the activated MR signatures [normalized enrichment score (NES) = 8.66, $P < 0.001$; Fig. 1E], demonstrating that the molecular drivers of mouse NPp53 CRPC are conserved with metastatic CRPC in humans.

Lastly, we asked whether molecular drivers of NPp53 CRPC are conserved specifically with those of human prostate tumors with reduced levels of *TP53* and *PTEN*. For this purpose, we generated two independent human MR signatures that compare cases having low *PTEN*/low *TP53* ($n = 5$) versus low *PTEN*/high *TP53* ($n = 5$) in primary tumors [from The Cancer Genome Atlas (TCGA)] and metastatic CRPC (from SU2C) (Supplementary Table S1; refs. 16, 17). We then performed cross-species GSEA using these human signatures to query the analogous mouse MR signature (NPp53 CRPC versus NP CRPC), which revealed a significant enrichment for both human MR signatures ($P < 0.001$; Fig. 1F; Supplementary Fig. S1B), indicating a high degree of molecular conservation of NPp53 CRPC-Adeno with human tumors having low *PTEN*/low *TP53*. Based on the histologic and molecular similarity of

NPp53 CRPC to human CRPC and particularly to CRPC with comutation of *TP53* and *PTEN*, we reasoned that these GEM models would be informative for preclinical investigations of treatment response for human CRPC.

Preclinical Analyses of Abiraterone Reveal Acceleration of the Tumor Phenotype in NPp53 CRPC

Although abiraterone is widely used for treatment of advanced prostate cancer (1), it has not been extensively investigated in preclinical studies *in vivo*. Furthermore, although originally described as a CYP17A1 inhibitor that blocks androgen biosynthesis, abiraterone has also been shown to be metabolized to a potent AR antagonist (29, 30), and thus can potentially inhibit androgen signaling at multiple levels. To perform preclinical studies, we first optimized dosing and scheduling parameters using strain-matched mice (Supplementary Fig. S2A–S2C), which led us to select a dose of 200 mg/kg/day, which is similar to the dosage used for other mouse strain backgrounds (e.g., ref. 31). Mass spectrometry analyses confirmed that abiraterone was both taken up and processed to its active form in wild-type mouse prostate as well as NPp53 CRPC (Supplementary Fig. S2C–S2D). However, because most of the relevant steroid metabolites are below or near the limits of detection of these assays, we were not able to determine whether the AR antagonist form (29, 30) is present in the mouse prostate.

Preclinical analyses revealed that response to treatment with abiraterone differed considerably between NP CRPC and NPp53 CRPC (Fig. 2A–E). In particular, abiraterone treatment resulted in a modest but significant inhibition of NP CRPC, as revealed by analyses of tumor histopathology, reduced cellular proliferation ($P = 0.006$, t test), and reduced tumor volume (an average of 12.5% decrease after treatment; $n = 15$ vehicle-treated and 21 abiraterone-treated; Fig. 2B–E, S3A; Supplementary Table S2). In contrast, NPp53 CRPC was not inhibited by abiraterone treatment, as evident from their histopathology and lack of reduced cellular proliferation or tumor volume following treatment ($n = 21$ vehicle-treated and 28 abiraterone-treated; Fig. 2B–E; Supplementary Fig. S3A–S2C; Supplementary Table S2). As it has been proposed that the consequences of p53 loss of function in prostate cancer are at least partially due to its inactivation in stroma (32), we examined whether the disparate effects of abiraterone treatment on NP and NPp53 CRPC could be attributed to non–cell-autonomous effects of stroma by generating epithelial cell lines from treatment-naïve tumors ($n = 2$ independent cell lines for each genotype; Supplementary Fig. S4A). The responses of these epithelial tumor cells to abiraterone *in vitro* and *in vivo* were analogous to those observed for the corresponding NP and NPp53 CRPC tumors (Supplementary Fig. S4B–S4D), indicating that the impaired response of NPp53 CRPC to abiraterone is, at least in part, cell autonomous.

Strikingly, not only did abiraterone treatment fail to reduce CRPC tumor growth in the NPp53 mice, a subset of these mice displayed accelerated tumor phenotypes following treatment. In particular, MRI analyses of NPp53 CRPC prior to and following abiraterone treatment revealed an approximately 2-fold increase in tumor volume after treatment (Supplementary Table S2). Furthermore, although some of the NPp53 CRPC mice analyzed by MRI had minimal change in volume (<10%), consistent with their lack of response to treatment ($n = 4/16$; Fig. 2D and E; Supplementary Table S2), most others displayed increased tumor volume (>10%) after treatment, in some cases up to 400% ($n = 12/16$; Fig. 2D and E; Supplementary Table S2); this difference was not due to differential tumor volumes prior to the initiation of treatment (Supplementary Fig. S3B–S3C). Moreover, although metastasis was rare in the NPp53 CRPC mice, several of the abiraterone-treated cases, but none of the vehicle-treated cases, displayed overt metastasis to visceral tissues; notably, these metastatic cases solely occurred in the NPp53 CRPC mice that displayed increased tumor volume by MRI ($n = 4/28$; Supplementary Table S2).

Furthermore, several of the NPp53 CRPC tumors displayed variant histologies, including areas of squamous, sarcomatoid, small-cell neuroendocrine-like, and other non-adenocarcinoma phenotypes, which were most prevalent in the abiraterone-treated NPp53 CRPC mice with increased tumor volume (Fig. 2B; Supplementary Fig. S5; Supplementary Tables S2 and S3). These areas of variant histopathology had reduced expression of AR and epithelial cytokeratins and significantly higher levels of proliferation (>50%) compared with regions of adenocarcinoma in the vehicle-treated mice ($P = 0.013$) or abiraterone-treated mice ($P = 0.03$; Fig. 2B and C; Supplementary Tables S2 and S3). Notably, similar regions of non-adenocarcinoma histopathology were observed in several of the vehicle-treated NPp53 CRPC tumors, as well as the intact (noncastrated) abiraterone-treated NPp53 mice (Supplementary Fig. S5; Supplementary Tables S2 and S3), suggesting that NPp53 CRPC has a latent potential for non-adenocarcinoma phenotypes that is augmented by abiraterone treatment.

To understand the molecular bases for their distinct phenotypic responses to abiraterone treatment, we performed expression profiling analyses comparing abiraterone- and vehicle-treated CRPC from the NP and NPp53 mice. Nonsupervised principal component analysis (PCA) showed that expression profiles from the abiraterone- and vehicle-treated NP CRPC clustered separately (Supplementary Fig. S6A), consistent with their phenotypic response to abiraterone. Furthermore, PCA using expression profiles from abiraterone-treated NPp53 CRPC tumors showed that a subset corresponding to those that did not display accelerated tumor phenotypes (Group 1) clustered with the vehicle-treated cases, consistent with their lack of phenotypic response to abiraterone treatment (Fig. 2F). However, the other abiraterone-treated NPp53 CRPC cases, corresponding to those that displayed accelerated tumor phenotypes (Group 2), were widely dispersed (Fig. 2F), indicating that this distinct phenotypic subgroup has divergent molecular profiles.

To investigate the diversity of response of these distinct subgroups of abiraterone-treated NPp53 CRPC to human CRPC, we performed single-sample GSEA (ssGSEA). In particular, we first compared each individual abiraterone-treated NP or NPp53 CRPC tumor sample with the pool of corresponding vehicle-treated tumors (NP or NPp53, respectively), defining a signature for each individual sample. We then performed cross-species ssGSEA comparing these individual signatures with a gene expression signature of human androgen-independent versus androgen-dependent prostate cancer from Best and colleagues (Supplementary Table S1; ref. 28). These analyses

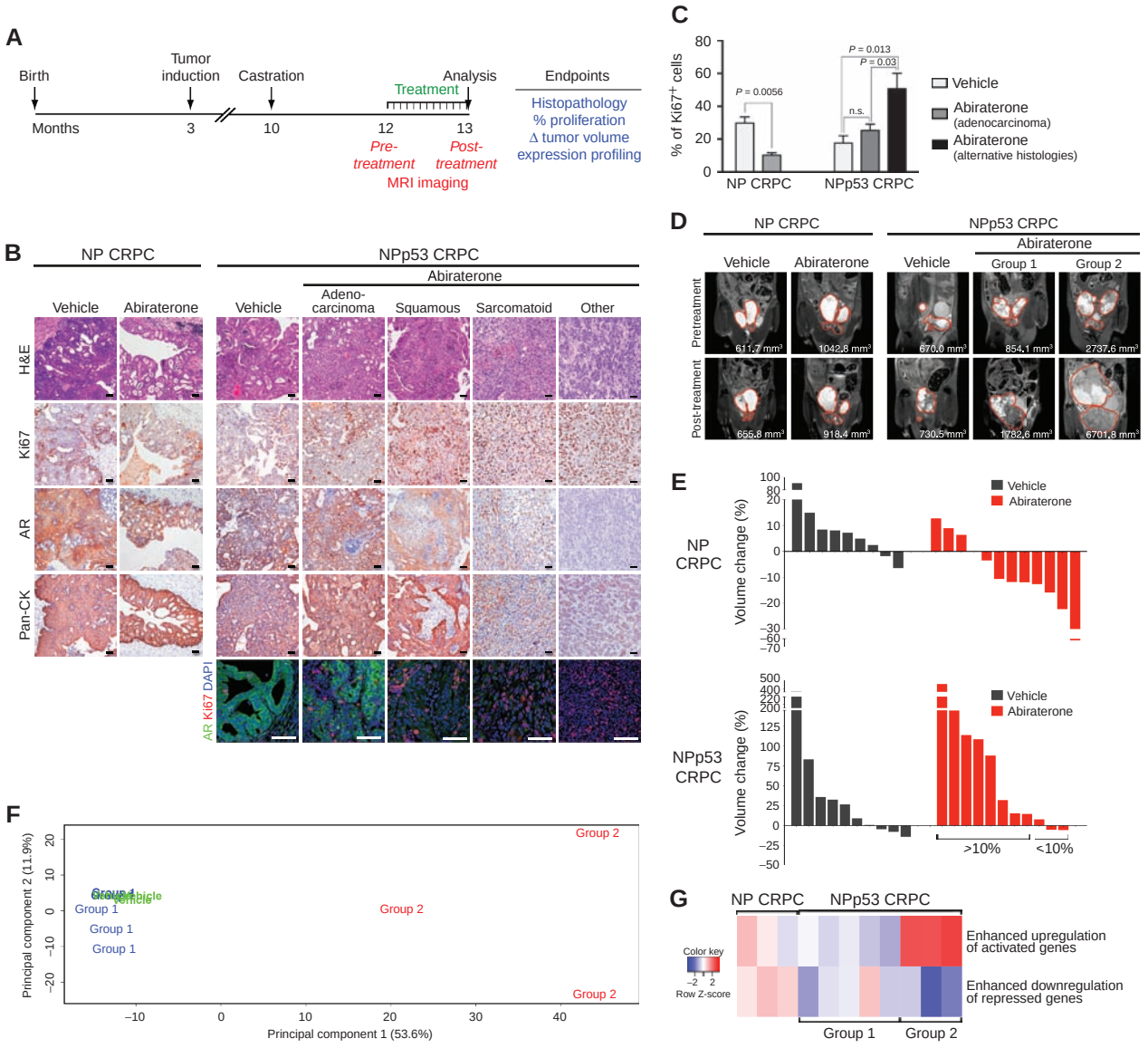

Figure 2. Preclinical analyses of abiraterone reveals acceleration of the tumor phenotype in NPp53 CRPC. **A,** Preclinical trial design. Tumors were induced in cohorts of NP or NPp53 mice by delivery of tamoxifen, and mice were subsequently castrated to induce CRPC. Mice were randomly assigned to the treatment or vehicle groups and treated with abiraterone-acetate (200 mg/kg) or vehicle 5 times weekly for 1 month. MRI was performed immediately prior to the first treatment and immediately after the last treatment. At the conclusion of the study, mice were sacrificed and tissues were collected for analysis, as indicated. **B,** Histologic phenotype of NP and NPp53 CRPC treated with vehicle or abiraterone. Shown are representative H&E images and immunohistochemical staining for the indicated antibodies. Abiraterone-treated NPp53 CRPC show representative examples of adenocarcinoma and alternative histopathologies, as in Supplementary Table S3. Scale bars, 50 μm. **C,** Quantification of cellular proliferation by analysis of Ki67 immunostaining. Data represent the average from five to eight independent images from three independent mice. *P* values indicate the difference between bracketed groups and were calculated by a *t* test. Note that cellular proliferation for the abiraterone-treated NPp53 CRPC was determined separately for regions of adenocarcinoma and alternative histopathologies. **D–E**, MRI analysis. The abiraterone-treated NPp53 CRPC show examples of Group 1 and Group 2 tumors, as described in the text. **D,** Representative images from 2-D MRI performed immediately prior to the first treatment (pretreatment) and immediately after the last treatment (post-treatment). Tumor volumes are indicated. **E,** Representative waterfall plots showing the change in tumor volume after treatment; each bar represents a single mouse. **F,** PCA based on comparison of RNA-sequencing gene expression profiles from NPp53 CRPC treated with vehicle (in green) or abiraterone (Group 1 in blue and Group 2 in red). **G,** Single-sample GSEA. Single-sample gene signatures were defined by comparing each individual abiraterone-treated NPp53 CRPC sample with the average of expression levels in the pooled group of corresponding vehicle-treated samples. Cross-species GSEA was performed to compare the single-sample signatures with a human gene signature of treatment-naïve androgen-independent versus androgen-dependent tumors of Best et al. (28). The comparison is shown as a heat map, wherein top and bottom boxes correspond to NESs from the GSEA between the single-sample reference signature and the top 200 overexpressed (top) and underexpressed (bottom) genes from the Best et al. signature (28). See also Supplementary Figs. S2–S6 for additional phenotypic and molecular analyses, Supplementary Table S2 for data summary, Supplementary Table S3 for quantitative analysis of the histopatholgy phenotypes, and Supplementary Dataset 1 for list of differentially expressed genes.

revealed that the group 2 abiraterone-treated NPp53 CRPC with accelerated tumor phenotypes has a strong positive enrichment in human CRPC, whereas the group 1 NPp53 CRPC and the NP CRPC were not strongly enriched (Fig. 2G).

Cross-Species Computational Analyses of Adverse Treatment Response

Our findings above define a subgroup of abiraterone-treated NPp53 CRPC with accelerated tumor phenotypes and distinct molecular profiles that are highly enriched for genes expressed in human CRPC. Based on their distinct histopathologic and molecular phenotypes, we term these group 2 abiraterone-treated NPp53 CRPC as "exceptional nonresponders" to distinguish them from the group 1 "nonresponder" NPp53 CRPC tumors and the "responder" NP CRPC tumors. Thus, in subsequent analyses, we consider these NPp53 CRPC "exceptional nonresponder" and "nonresponder" groups separately and compare these with the NP CRPC "responder" group.

In previous studies, we showed that cross-species analysis of treatment response in GEM models can identify candidate molecular drivers (MRs) that are informative for stratifying human patients based on treatment response and/or disease outcome (33). In particular, we showed that expression profiles comparing pretreatment versus posttreatment of GEM models can be used as a quantitative measure of drug response, such that treatments that inhibit tumor phenotypes (in "responders") result in reversion of the MR signatures in the posttreatment group, which can be quantified by the downregulation of activated target genes and upregulation of repressed target genes (Fig. 3A, scenario 1; ref. 33). In contrast, "nonresponders" are phenotypically and molecularly similar to the vehicle-treated controls and have signatures that are essentially unchanged after treatment (Fig. 3A, scenario 2). By extension of this logic, we hypothesized that "exceptional nonresponders" would display an enhancement of the MR signature (Fig. 3A, scenario 3), which might be associated with adverse treatment response and/or adverse disease outcome in human CRPC.

To test this concept, we performed cross-species analyses to query MR signatures from relevant human CRPC datasets, using reference signatures based on these distinct groups of "responder," "nonresponder," and "exceptional nonresponder" mouse tumors. In particular, we performed MARINa to generate mouse MR signatures corresponding to (i) the "responder" abiraterone- versus vehicle-treated NP tumors (scenario 1); (ii) the "nonresponder" (group 1) abiraterone- versus vehicle-treated NPp53 tumors (scenario 2); and (iii) the "exceptional nonresponder" (group 2) abiraterone- versus vehicle-treated NPp53 tumors (scenario 3). We then performed cross-species GSEA using each of these reference mouse MR signatures to query two independent human CRPC MR signatures: (i) a signature comparing bone metastases from CRPC with hormone-naïve prostate primary tumors from the Balk dataset (34), and (ii) a signature comparing androgen-independent and androgen-dependent prostate tumors from the Best dataset, as described above (Supplementary Table S1; ref. 28).

We found that the MR signature of the "exceptional nonresponder" NPp53 tumors was strongly positively enriched in the human MR signatures from both the Balk (NES = 7.22, $P < 0.001$) and Best (NES = 5.12, $P < 0.001$) datasets (Fig. 3B; Supplementary Fig. S6B). In contrast, the MR signature of "responder" NP tumors was reverted in both human MR signatures (Balk NES = 7.45, $P < 0.001$; Best NES = 7.79, $P < 0.001$), whereas the "nonresponder" NPp53 signature displayed minimal enrichment in either human MR signature (Fig. 3B; Supplementary Fig. S6B). These findings are consistent with our predictions (Fig. 3A) and indicate that the exceptional nonresponders have molecular drivers that are conserved with human CRPC.

To extend these analyses to treatment response, we generated a human MR signature comparing CRPC tumors with neuroendocrine differentiation (CRPC-NE; $n = 15$), most of which were treatment-related, to CRPC tumors with adenocarcinoma (CRPC-Adeno; $n = 34$), as reported by Beltran and colleagues (5). We queried this human signature with a mouse MR signature comparing the "exceptional nonresponder" abiraterone-treated NPp53 tumors to the "responder" NP tumors, which revealed a significant enrichment in both the upregulated and downregulated MRs (NES = 3.36, $P = 0.006$, and NES = −4.03, $P < 0.001$, respectively; Fig. 3C). These findings indicate strong conservation of adverse treatment response in mouse CRPC with drivers of treatment failure and neuroendocrine differentiation in human prostate cancer and identify conserved MRs that drive the CRPC-NE phenotype, which we refer to as "adverse treatment response MRs" (Supplementary Table S4). To evaluate whether these adverse treatment response MRs are associated with disease outcome, we used the Sboner and colleagues dataset, which is one of the few published cohorts with extensive clinical outcome data, including disease-specific death due to prostate cancer (Supplementary Table S1; ref. 35). Kaplan–Meier survival analysis using this dataset revealed that patients with higher activity levels of the adverse treatment-response MRs had a shorter time to prostate cancer–specific death compared with those with lower activity levels (log-rank $P = 8.32 \times 10^{-6}$; Fig. 3D), providing clinical validation that these adverse treatment response MRs are relevant for disease outcome in human prostate cancer.

Cumulatively, these phenotypic and computational analyses define a subgroup of "exceptional nonresponders" in the mouse that are conserved with more aggressive variants of human CRPC, including CRPC-NE. Furthermore, the molecular drivers of this phenotype, namely the adverse treatment-response MRs, are conserved with human CRPC, enriched in patients who develop CRPC-NE, and associated with adverse outcome for human prostate cancer. Therefore, these adverse treatment-response MRs may help identify patients with aggressive prostate cancer and/or who are predisposed to fail treatment with abiraterone.

Neuroendocrine Differentiation in *TP53*-Deficient CRPC Is Mediated in Part by *SOX11*

These findings suggest that the treatment-related NPp53 CRPC phenotype shares molecular features in common with human CRPC-NE. Indeed, we found that expression profiles of NPp53 "exceptional nonresponders" displayed significant dysregulation of genes that have been shown to be expressed in human CRPC-NE (ref. 6; $P < 0.05$, t test; Fig. 4A). Therefore, we queried the adverse treatment response MRs (Supplementary Table S4) to identify candidate MRs that might contribute

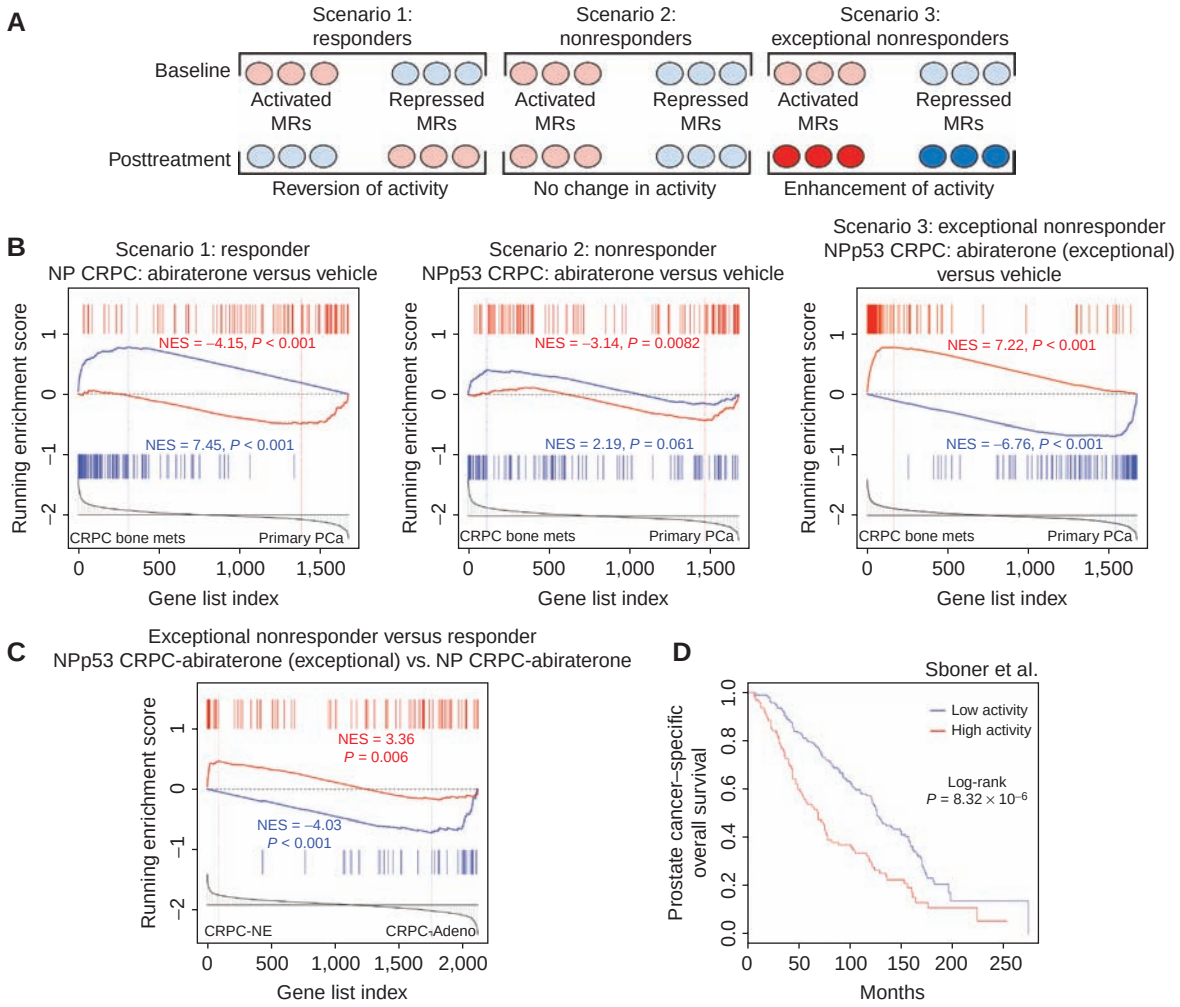

Figure 3. Cross-species computational analyses of adverse treatment response. **A,** Schematic diagram showing the computational strategy used to predict molecular drivers of adverse treatment response. Illustrated are three possible outcomes: In scenario 1, the "responder" group, drug treatment is predicted to reverse the direction of MR signatures [i.e., activated MRs (red) are repressed (blue) and vice versa]. In scenario 2, the "nonresponder" group, drug treatment is predicted to have minimal effect on MR signatures. In scenario 3, the "exceptional nonresponder" group, drug treatment is predicted to enhance the activation or repression of MR signatures [i.e., activated red MRs (red) are further activated (darker red) and repressed MRs (blue) are further repressed (darker blue)]. **B** and **C,** Cross-species GSEA. **B,** The reference signature, a human MR signature from Balk et al. (34) comparing CRPC bone metastasis (mets; $n = 29$) versus primary hormone-naïve prostate tumors (PCa; $n = 22$), was compared with three independent mouse MR query signatures from abiraterone- versus vehicle-treated "responders" (NP CRPC), "nonresponders" (NPp53 CRPC, Group 1), or "exceptional nonresponders" (NPp53 CRPC, Group 2). **C,** The reference signature, a human MR signature from Beltran et al. (5) comparing CRPC-NE ($n = 15$) with CRPC-Adeno ($n = 34$), was compared with a mouse MR query signature comparing abiraterone-treated "exceptional nonresponders" (NPp53 CRPC, Group 2) versus abiraterone-treated "responders" (NP CRPC). In **B** and **C,** NES and *P* values were calculated using 1,000 gene permutations. **D,** Kaplan–Meier survival analysis was estimated based on the activity levels of adverse treatment response MRs (as in panel **C** and Supplementary Table S4) based on Sboner et al. (35) using prostate cancer–specific survival as the endpoint ($n = 281$ patients). The *P* value was estimated using a log-rank test to determine the difference in outcomes between patients with higher activity levels of adverse treatment response MR (red) and those with lower/no MR activity (blue). See also Supplementary Fig. S6 for additional analyses, Supplementary Table S1 for description of human datasets, and Supplementary Table S4 for summary of MRs identified in **C**.

to the CRPC-NE phenotype. Among these, we focused on *SOX11*, a member of the SOXC subclass of HMG-box transcriptional regulators that functions in a wide range of neural and mesenchymal progenitors during organogenesis and is also a pan-neuronal differentiation factor (36–38). Notably, *SOX11* has been shown to be regulated by *TP53* in other contexts (39), and was one of the top upregulated genes between mouse NP and NPp53 CRPC ($P = 0.0003$, *t* test; dataset 1). Furthermore, *Sox11* was among the most upregulated genes in the TRAMP mouse model of prostate cancer in the transition from adenocarcinoma to neuroendocrine disease (40).

We found that *SOX11* expression is significantly upregulated in comparing higher versus lower Gleason grade primary tumors ($P = 0.028$, *t* test), as reported by TCGA (16), as well as in CRPC-NE relative to CRPC-Adeno ($P = 0.012$, *t* test), as reported by Beltran and colleagues (ref. 5; Fig. 4B). Furthermore, target genes that are predicted to be upregulated by SOX11 in the human prostate cancer interactome are significantly enriched in CRPC-NE versus CRPC-Adeno (NES 4.31, $P < 0.001$; Fig. 4C). We found that *Sox11* mRNA expression was also upregulated in mouse NPp53 CRPC relative to NP CRPC ($P < 0.01$, *t* test), and particularly in the exceptional

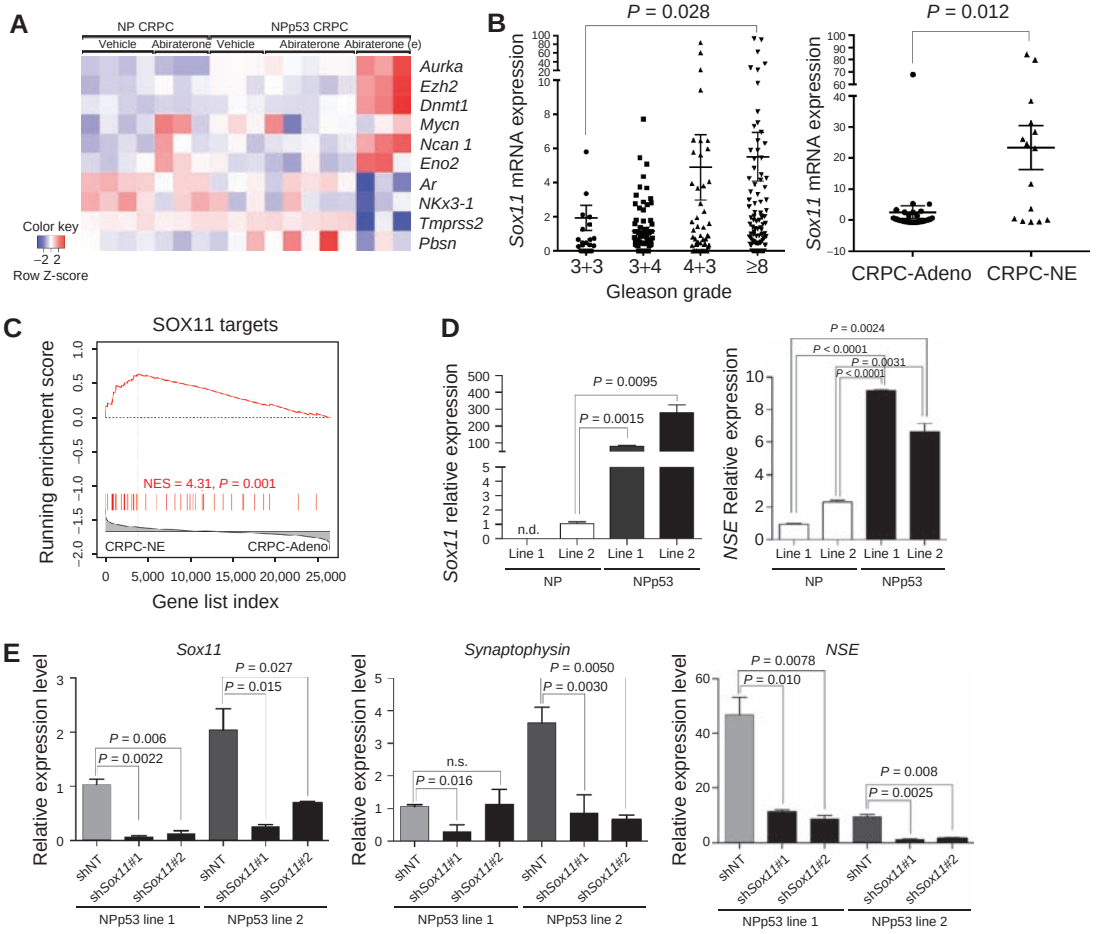

Figure 4. Neuroendocrine differentiation in *TP53*-deficient CRPC is mediated in part by *SOX11*. **A,** Heat map depicting relative expression levels of genes associated with neuroendocrine differentiation in vehicle- or abiraterone-treated mouse CRPC (6). e, exceptional nonresponders. **B,** Relative expression level of *SOX11* in human prostate cancer showing primary tumors segregated by Gleason grade (from TCGA) or CRPC-Adeno versus CRPC-NE (5). **C,** GSEA showing the enrichment of *SOX11* target genes, predicted from analyses of a human prostate cancer interactome, in a human signature comparing CRPC-Adeno or CRPC-NE (5). NES and *P* value were calculated using 1,000 gene permutations. **D,** Quantitative real-time PCR showing expression levels of *Sox11* and neuron-specific enolase (NSE) in two independent mouse prostate epithelial cell lines from NP or NPp53 tumors (see Supplementary Fig. S4). **E,** Expression levels of *Sox11*, *NSE*, and *Synaptophysin* in mouse NPp53 cell lines following knock-down using two independent shRNA for *Sox11* (sh*Sox11*#1 and sh*Sox11*#2). shNT is the nontargeting control vector. In **B, D,** and **E,** *P* values were calculated using a *t* test.

nonresponders (Supplementary Fig. S7A). In addition, *Sox11* expression was upregulated in mouse epithelial cell lines established from these NPp53 tumors relative to lines from NP tumors ($P < 0.01$, *t* test), and was correlated with expression of the neuroendocrine marker neuron-specific enolase (NSE; $P < 0.01$, *t* test; Fig. 4D). Furthermore, we found that shRNA-mediated knockdown of *Sox11* in the NPp53 mouse cell lines resulted in downregulation of neuroendocrine markers, such as *NSE* and *Synaptophysin* ($P < 0.02$, *t* test; Fig. 4E), while not resulting in reduced expression of other *Sox* genes, such as *Sox2* or *Sox7* (Supplementary Fig. S7B). Taken together, these findings suggest that neuroendocrine differentiation in treatment-related NPp53 CRPC is mediated at least in part by *Sox11*.

Focal and Overt Neuroendocrine Differentiation Arise through Transdifferentiation of Luminal Prostate Epithelial Cells

Given these molecular findings showing that NPp53 CRPC shares features in common with human CRPC-NE, we investigated whether the NPp53 CRPC tumors display neuroendocrine differentiation by immunostaining for Synaptophysin, a neuroendocrine marker that is rarely expressed in hormonally intact prostate adenocarcinoma. In particular, we determined the relative abundance of Synaptophysin-positive (Syn^+) cells in tumors from NP and NPp53 mice that were hormonally intact, castrated, or castrated with abiraterone treatment (Fig. 5A and B; Supplementary Table S5A). Although Syn^+ cells were very rare in *NP* tumors in all cases (less than 1% in all contexts, $n = 3$ to 7/group) as well as in NPp53 intact tumors (0.34%; $n = 7$, one-way ANOVA), they were significantly more abundant in both the castrated (2.54%; $n = 11$; $P < 0.05$, one-way ANOVA) and castrated and abiraterone-treated NPp53 mice (4.03%; $n = 12$, $P < 0.001$, one-way ANOVA). In some cases, however, the Syn^+ cells were extremely abundant, comprising up to 99% of the total cells in the region (Fig. 5B and C; Supplementary Table S5A).

In the nonresponder mice, we mostly observed small patches of Syn^+ cells within regions of adenocarcinoma (Fig. 5A),

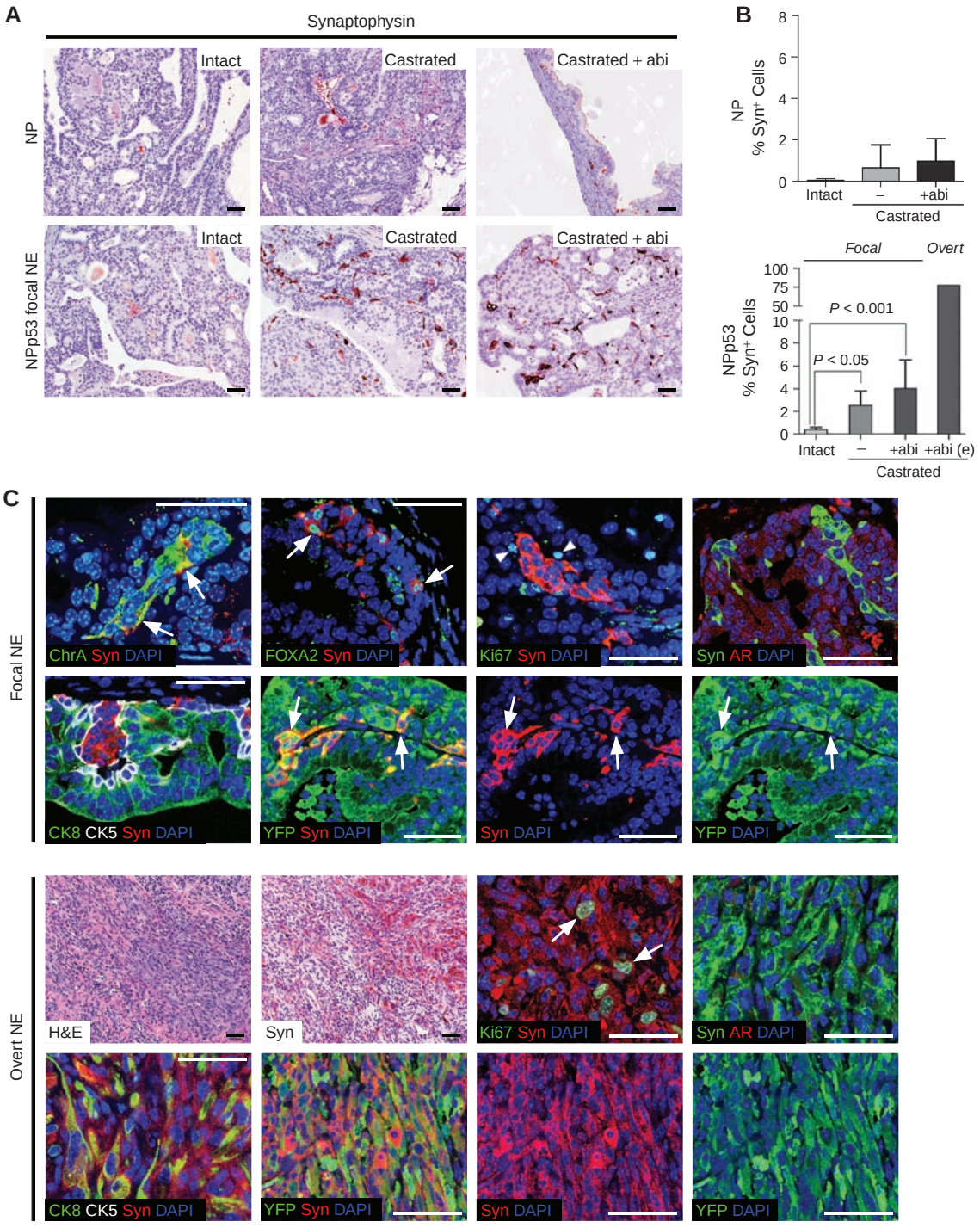

Figure 5. Focal and overt neuroendocrine differentiation arise through transdifferentiation of luminal cells. **A,** Immunostaining for Synaptophysin (Syn) in intact or castrated NP and NPp53 tumors treated with vehicle or abiraterone (abi), as indicated. Shown are regions of focal neuroendocrine differentiation. Scale bars, 50 μm. **B,** Quantification of the percentage of Synaptophysin positive (Syn+) cells in regions of focal and overt neuroendocrine differentiation. Data quantification is provided in Supplementary Table S5. *P* values were calculated by one-way ANOVA. e, exceptional nonresponders. **C,** Histologic phenotype of lineage-marked Synaptophysin+ cells in regions of focal and overt NPp53 CRPC. Shown is representative immunostaining for the indicated antibodies. Data quantification are provided in Supplementary Table S5. Scale bars, 50 μm.

consistent with focal neuroendocrine differentiation. These Syn$^+$ cells also coexpressed other neuroendocrine markers such as Chromogranin A and FOXA2; they also expressed the luminal marker cytokeratin 8 (CK8), albeit at lower levels, but not the basal cell marker CK5, and expressed low levels of AR compared with the surrounding non-Syn$^+$ cells (Fig. 5C). Notably, in these regions of focal neuroendocrine differentiation in castrated or castrated plus abiraterone-treated mice, the Syn$^+$ cells

never coexpressed the proliferation marker Ki67 (0/357 and 0/560 cells, respectively; Fig. 5C; Supplementary Table S5B).

In contrast, exceptional nonresponder tumors displayed some regions in which Syn$^+$ cells comprised the bulk of tumor cells (>70% of tumor cells; Fig. 5C; Supplementary Table S5B). In these regions of overt neuroendocrine differentiation, the Syn$^+$ cells phenotypically resemble those found in focal differentiation, but were completely lacking AR expression (Fig. 5C). Notably, however, the Syn$^+$ cells in areas of overt neuroendocrine differentiation are highly proliferative, as shown by Ki67 coexpression (44%, $n = 461/1038$ Ki67 positive cells; Fig. 5C; Supplementary Table S5B).

Finally, we sought to determine the cellular origin of the Syn$^+$ cells in both the focal and overt regions of neuroendocrine differentiation. For this purpose, we performed lineage tracing using NPp53 mice that also carried a *R26R-YFP* reporter allele. As the inducible *Nkx3.1*^{CreERT2} driver is specific for luminal epithelial cells in the adult prostate (19, 22), YFP is expressed only by luminal cells and their descendants in NPp53 tumors. We found that nearly all Syn$^+$ cells in NPp53 tumors coexpressed YFP, demonstrating that these Syn$^+$ cells were derived from luminal cells, and not from neuroendocrine or basal cells ($n = 346/347$ cells; Fig. 5C; Supplementary Table S5B). Furthermore, this was the case for Syn$^+$ cells in both the focal and overt regions of neuroendocrine differentiation ($n = 519/521$ in the latter; Fig. 5C; Supplementary Table S5B), despite the considerable differences in the proliferative status of the Syn$^+$ cells and tumor phenotype between these groups. Therefore, these findings provide direct genetic evidence in a mouse model of CRPC-NE that both focal and overt neuroendocrine differentiation arises by transdifferentiation of luminal prostate adenocarcinoma cells.

DISCUSSION

The elucidation of the biological and molecular processes that underlie adverse treatment response and identification of patients that are likely to fail treatment represent fundamental clinical challenges that are particularly germane for prostate cancer. In the current study, we have used an integrative approach that combines phenotypic and molecular analyses of mouse and human CRPC to investigate the underlying causes of treatment failure for abiraterone, an antiandrogen that is now widely used in the clinic (1). Our findings demonstrate that the NPp53 mouse model of CRPC recapitulates key phenotypic and molecular characteristics of human CRPC. Furthermore, preclinical analyses of NPp53 CRPC reveal that these tumors fail to respond to abiraterone, suggesting that CRPC with coinactivation of *PTEN* and *TP53,* which is frequent in humans, may be inherently less responsive to abiraterone. Moreover, we observed that many of the NPp53 CRPC tumors were actually accelerated in their phenotype by abiraterone treatment. These "exceptional nonresponders" display highly aggressive histopathologic phenotypes that share molecular and phenotypic features in common with treatment-related CRPC-NE in humans (Fig. 6). Furthermore, cross-species computational analysis has identified treatment response regulators that are associated with adverse disease outcome in human CRPC-NE, which may enable identification of patients prior to treatment who are at risk for developing CRPC-NE.

To date, it has been unclear whether focal versus overt neuroendocrine differentiation in CRPC represents two distinct entities at the phenotypic and/or molecular level. Although neuroendocrine differentiation is rare in primary prostate cancer, it can be occasionally observed in CRPC as sporadic small foci of cells expressing neuroendocrine markers (41, 42). However, the recent widespread clinical use of antiandrogens has been selected for the emergence of CRPC-NE, which features large regions of overt neuroendocrine differentiation typically having small-cell histology and neuroendocrine marker expression (4, 5). Our current results model focal and overt neuroendocrine differentiation in the "nonresponder" and "exceptional nonresponder" NPp53 CRPC mice, respectively. We find that a distinguishing feature of focal neuroendocrine differentiation is that the neuroendocrine-like cells are nonproliferative, in striking contrast to overt neuroendocrine differentiation, which is highly proliferative. On the basis of these observations, we suggest that a stochastic event during tumor progression promotes proliferation of neuroendocrine-like cells, which are consequently selected by abiraterone treatment as they completely lack AR expression (Fig. 6). We propose that such a "proliferative switch" might represent a key molecular event in the emergence of CRPC-NE.

Our study provides new insights into the roles of *TP53* and *PTEN*, and their relationship to other relevant drivers, in suppressing cellular plasticity and neuroendocrine differentiation in prostate cancer, which is significant because comutation of *TP53* and *PTEN* is considerably more prevalent than that of *RB* and *TP53* in advanced prostate cancer. Indeed,

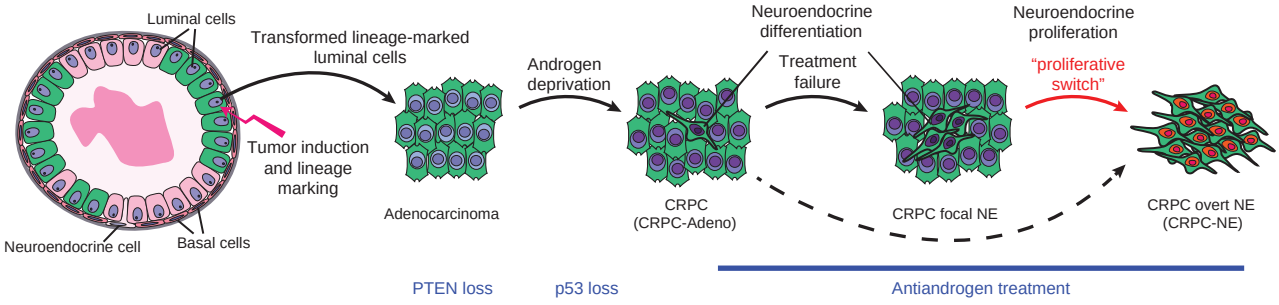

Figure 6. This model depicts the molecular and phenotypic events associated with progression to CRPC, including treatment failure and transdifferentiation to CRPC-NE. The model is further described in the text.

previous studies have reported that dysregulation of *TP53* and/or *RB* and/or *PTEN* is associated with the transition to small-cell neuroendocrine-like tumors in human prostate cancer (7, 59). Notably, there has been little precedent for a role of PTEN in modulating cellular plasticity, which deserves further investigation. In contrast, a general role for the p53 pathway in regulating cellular reprogramming has been previously suggested by studies showing that inhibition of p53 pathway activity results in increased efficiency in the formation of induced pluripotent stem cells (43–47). Moreover, the specific functional relevance of *RB* and *TP53* in neuroendocrine differentiation has been previously demonstrated in a GEM model based on their combined loss of function (24), as well as in the TRAMP and LADY mouse models, in which inactivation of *RB* and *TP53* results in adenocarcinoma and neuroendocrine differentiation (48, 49). In the current study, we find that *Rb1* is significantly reduced in expression in NPp53 CRPC and particularly in those cases with overt neuroendocrine differentiation (Supplementary Fig. S7A). Furthermore, two recent studies have shown that combined loss of *RB* and *TP53* in human and mouse models leads to altered sensitivity to antiandrogen treatment and upregulation of *SOX2,* which promotes epithelial plasticity (50, 51). Interestingly, combined loss of *RB* and *TP53* facilitates neuroendocrine differentiation via upregulation of *SOX2* in a model of small-cell lung cancer (52), suggesting that there may be common mechanisms in the transition to neuroendocrine disease across cancer types.

The findings of our study suggest that *SOX11*, a known target of *TP53*, is likely to be a key modulator of neuroendocrine differentiation in CRPC-NE. Notably, distinct SOX transcription factors are believed to act sequentially during neurogenesis, with members of the SOXB1 subclass such as SOX2 functioning to maintain the neural progenitor state and inhibit differentiation, whereas SOXC factors such as SOX11 function later to promote neuronal differentiation (36, 53). By analogy, we propose that SOX2 may act early in the emergence of CRPC-NE to promote epithelial plasticity (51), whereas SOX11 may act at subsequent stages to promote neuroendocrine differentiation. Interestingly, we find that *Sox2* expression is reduced in the NPp53 CRPC relative to *NP* CRPC (Supplementary Fig. S7A). Among the predicted targets of SOX11 are *POU3F2* (*BRN2*), which can drive a neuroendocrine phenotype in prostate cancer xenografts (54), as well as *MYCN* (6), which promotes the formation of a CRPC-NE phenotype in relevant human and mouse models in collaboration with *Pten* loss of function or activation of AKT kinase activity (55, 56). Interestingly, these activities of *Mycn* contrast with those of *Myc* (*c-Myc*), which collaborates with *Pten* loss of function in mouse models to generate highly aggressive adenocarcinoma and metastasis but not neuroendocrine differentiation (57).

Our analyses provide definitive and quantitative evidence that both focal and overt neuroendocrine differentiation in prostate cancer occurs through transdifferentiation from luminal tumor cells (Fig. 6). In particular, we have demonstrated transdifferentiation by lineage tracing, which represents the "gold standard" approach for analyses of cell fate specification *in vivo* (58). Thus, our findings extend and greatly strengthen the conclusions of previous work that had suggested that CRPC-NE arises from luminal adenocarcinoma cells, based on sequence analyses and detection of the *TMPRSS2–ERG* translocation by fluorescent *in situ* hybridization (5, 6, 59). Furthermore, the common origin of both focal and overt neuroendocrine differentiation from luminal cells may be consistent with a linear pathway for their emergence (Fig. 6). However, it remains conceivable that focal versus overt neuroendocrine differentiation can arise from distinct luminal subpopulations within CRPC-Adeno tumors.

Interestingly, transdifferentiation has been implicated as a potential cause of drug resistance in a clinical setting for non–small cell lung cancer with alterations of *TP53* and *RB1* (60, 61). Our current findings provide direct experimental evidence for transdifferentiation in mediating drug resistance, and extend the generality of this mechanism to other tumor types and cancer drivers. Thus, perturbations of key conserved pathways that regulate cellular plasticity and differentiation in normal developmental contexts may represent significant mechanisms for driving drug resistance in cancer.

METHODS

Preclinical and Phenotypic Analyses of GEM Models

All experiments using animals were conducted according to protocols approved by the Institutional Animal Care and Use Committee at Columbia University Medical Center. Mouse alleles were obtained from the NCI Mouse Models of Human Cancer Consortium Repository (http://mouse.ncifcrf.gov/) or The Jackson Laboratory (https://www.jax.org) and maintained in a mixed C57BL/6/129S strain background. Abiraterone-acetate was provided by Johnson & Johnson. Optimal dosage, pharmacokinetic profile, and optimal scheduling were determined using non–tumor-bearing littermates (Supplementary Fig. S2). Preclinical studies were done using tamoxifen-induced NP and NPp53 mice that had been surgically castrated. Treatment was initiated 2 months after castration and continued for 4 weeks following which prostate tissues were collected for analyses (see detailed experimental procedures in the Supplementary Materials).

Semiquantitative analysis of histologic phenotypes is summarized in Supplementary Table S3. Immunostaining was done as described (22); quantification was done using at least five sections per mouse and from at least three independent mice per group, and summarized in Supplementary Table S5. MRI was done using a Bruker Biospec 9.4T Tesla Small Animal MR Imager. Levels of steroids and abiraterone in prostate tissues and serum were determined by mass spectrometry. Allograft studies were done using cell lines generated from treatment-naïve NP or NPp53 tumors (see detailed experimental procedures in Supplementary Materials), which were implanted into the flanks of immunodeficient NCr nude mice (Taconic) followed by treatment with abiraterone. All antibodies used for this study are provided in Supplementary Table S6; all primers are described in Supplementary Table S7.

Gene Expression Profiling and Computational Analyses

Gene expression profiling of mouse CRPC was done using RNA sequencing on an Illumina HiSeq 2500 platform; a complete list of differentially expressed genes is provided in Supplementary Dataset 1. Published human datasets used in these studies for cross-species analyses are described in Supplementary Table S1. Master regulator analysis was performed using MARINa to interrogate a human prostate cancer interactome, as described (27). Cross-species gene GSEA and ssGSEA were done using "humanized" mouse signatures and human MR signatures, as described (27).

Statistical Analyses

Statistical analyses were performed using a two-tailed *t* test, one-way ANOVA, χ^2 test, and Fisher exact test as appropriate. GraphPad Prism software (Version 6.0) and R-studio 0.99.902, R v3.3.0, were used for statistical calculations and data visualization. COX proportional hazard model and Kaplan–Meier analysis were done with the surv and coxph functions from survcomp package (Bioconductor).

Accession Numbers

Mouse expression profiling data are deposited in the Gene Expression Omnibus (GEO) database (GSE92721).

Disclosure of Potential Conflicts of Interest

A. Califano is Cofounder and Chief Scientific Advisor at DarwinHealth, Inc., and has ownership interest (including patents) in DarwinHealth, Inc. No potential conflicts of interest were disclosed by the other authors.

Authors' Contributions

Conception and design: M. Zou, R. Toivanen, N. Floch, D. Chester, M.M. Shen, C. Abate-Shen

Development of methodology: M. Zou, R. Toivanen, A. Mitrofanova, N. Floch, Y. Sun, C. Le Magnen, D. Chester

Acquisition of data (provided animals, acquired and managed patients, provided facilities, etc.): M. Zou, R. Toivanen, N. Floch, Y. Sun, C. Le Magnen, D. Chester, E.A. Mostaghel

Analysis and interpretation of data (e.g., statistical analysis, biostatistics, computational analysis): M. Zou, R. Toivanen, A. Mitrofanova, N. Floch, S. Hayati, Y. Sun, D. Chester, E.A. Mostaghel, A. Califano, M.A. Rubin, M.M. Shen, C. Abate-Shen

Writing, review, and/or revision of the manuscript: M. Zou, R. Toivanen, A. Mitrofanova, Y. Sun, C. Le Magnen, E.A. Mostaghel, M.M. Shen

Administrative, technical, or material support (i.e., reporting or organizing data, constructing databases): N. Floch

Study supervision: N. Floch, A. Califano, M.M. Shen, C. Abate-Shen

Grant Support

We thank Johnson & Johnson for the gift of the abiraterone–acetate. We acknowledge support from the JP Sulzberger Columbia Genome Center and the Small Animal Imaging Facility, which are shared resources of the Herbert Irving Comprehensive Cancer Center at Columbia University, supported in part by NIH/NCI grant #P30 CA013696, and the Biomarkers Core Laboratory at Columbia University Medical Center, which is supported by the National Center for Advancing Translational Sciences, National Institutes of Health, Grant Number UL1 TR000040. The Steroid Analyses Core at the Fred Hutchinson Cancer Research Center is supported by the Pacific Northwest Prostate Cancer SPORE P50CA097186 and P01 CA163227. This research was supported by funding from the National Cancer Institute to C. Abate-Shen (CA173481), M.M. Shen (CA154293 and DK076602), M.M. Shen and C. Abate-Shen (CA196662), A. Califano and C. Abate-Shen (U54 CA209997), and A. Califano (R35 CA197745); from the DOD Prostate Cancer Research Program to M.M. Shen (PC150051); and from the Prostate Cancer Foundation and the TJ Martell Foundation for Leukemia, Cancer and AIDS Research. M. Zou was supported in part by the National Center for Advancing Translational Sciences, National Institutes of Health, Grant Number UL1TR001873. R. Toivanen was supported by grants from the DOD Prostate Cancer Research Program (PC131821) and an Early Career Fellowship from the National Health and Medical Research Council of Australia (1090204). C. Le Magnen was supported by the Swiss National Science Foundation (PBBSP3_146959 and P300P3_151158). A. Mitrofanova was a recipient of a Prostate Cancer Foundation Young Investigator Award. N. Floch was supported by an AACR–Millennium Fellowship in Prostate Cancer Research. C. Abate-Shen is an American Cancer Society Research Professor supported in part by a generous gift from the F.M. Kirby Foundation.

The costs of publication of this article were defrayed in part by the payment of page charges. This article must therefore be hereby marked *advertisement* in accordance with 18 U.S.C. Section 1734 solely to indicate this fact.

Received October 18, 2016; revised November 14, 2016; accepted April 12, 2017; published OnlineFirst April 14, 2017.

REFERENCES

1. Attard G, Parker C, Eeles RA, Schroder F, Tomlins SA, Tannock I, et al. Prostate cancer. Lancet 2016;387:70–82.
2. Scher HI, Solo K, Valant J, Todd MB, Mehra M. Prevalence of prostate cancer clinical states and mortality in the united states: estimates using a dynamic progression model. PLoS One 2015;10:e0139440.
3. Scher HI, Sawyers CL. Biology of progressive, castration-resistant prostate cancer: directed therapies targeting the androgen-receptor signaling axis. J Clin Oncol 2005;23:8253–61.
4. Watson PA, Arora VK, Sawyers CL. Emerging mechanisms of resistance to androgen receptor inhibitors in prostate cancer. Nat Rev Cancer 2015;15:701–11.
5. Beltran H, Prandi D, Mosquera JM, Benelli M, Puca L, Cyrta J, et al. Divergent clonal evolution of castration-resistant neuroendocrine prostate cancer. Nat Med 2016;22:298–305.
6. Beltran H, Rickman DS, Park K, Chae SS, Sboner A, MacDonald TY, et al. Molecular characterization of neuroendocrine prostate cancer and identification of new drug targets. Cancer Discov 2011;1:487–95.
7. Aparicio AM, Shen L, Tapia EL, Lu JF, Chen HC, Zhang J, et al. Combined tumor suppressor defects characterize clinically defined aggressive variant prostate cancers. Clin Cancer Res 2016;22:1520–30.
8. Aggarwal R, Zhang T, Small EJ, Armstrong AJ. Neuroendocrine prostate cancer: subtypes, biology, and clinical outcomes. J Natl Compr Canc Netw 2014;12:719–26.
9. Humphrey PA. Histological variants of prostatic carcinoma and their significance. Histopathology 2012;60:59–74.
10. Berman-Booty LD, Knudsen KE. Models of neuroendocrine prostate cancer. Endocr Relat Cancer 2015;22:R33–49.
11. Terry S, Beltran H. The many faces of neuroendocrine differentiation in prostate cancer progression. Front Oncol 2014;4:60.
12. Taylor BS, Schultz N, Hieronymus H, Gopalan A, Xiao Y, Carver BS, et al. Integrative genomic profiling of human prostate cancer. Cancer Cell 2010;18:11–22.
13. Baca SC, Prandi D, Lawrence MS, Mosquera JM, Romanel A, Drier Y, et al. Punctuated evolution of prostate cancer genomes. Cell 2013;153:666–77.
14. Barbieri CE, Baca SC, Lawrence MS, Demichelis F, Blattner M, Theurillat JP, et al. Exome sequencing identifies recurrent SPOP, FOXA1 and MED12 mutations in prostate cancer. Nat Genet 2012;44:685–9.
15. Grasso CS, Wu YM, Robinson DR, Cao X, Dhanasekaran SM, Khan AP, et al. The mutational landscape of lethal castration-resistant prostate cancer. Nature 2012;487:239–43.
16. Network CGAR. The molecular taxonomy of primary prostate cancer. Cell 2015;163:1011–25.
17. Robinson D, Van Allen EM, Wu YM, Schultz N, Lonigro RJ, Mosquera JM, et al. Integrative clinical genomics of advanced prostate cancer. Cell 2015;161:1215–28.
18. Fraser M, Sabelnykova VY, Yamaguchi TN, Heisler LE, Livingstone J, Huang V, et al. Genomic hallmarks of localized, non-indolent prostate cancer. Nature 2017;541:359–64.
19. Wang X, Kruithof-de Julio M, Economides KD, Walker D, Yu H, Halili MV, et al. A luminal epithelial stem cell that is a cell of origin for prostate cancer. Nature 2009;461:495–500.
20. Chen Z, Trotman LC, Shaffer D, Lin HK, Dotan ZA, Niki M, et al. Crucial role of p53-dependent cellular senescence in suppression of Pten-deficient tumorigenesis. Nature 2005;436:725–30.

21. Lunardi A, Ala U, Epping MT, Salmena L, Clohessy JG, Webster KA, et al. A co-clinical approach identifies mechanisms and potential therapies for androgen deprivation resistance in prostate cancer. Nat Genet 2013;45:747–55.
22. Toivanen R, Mohan A, Shen MM. Basal progenitors contribute to repair of the prostate epithelium following induced luminal anoikis. Stem Cell Rep 2016;6:660–7.
23. Wang ZA, Toivanen R, Bergren SK, Chambon P, Shen MM. Luminal cells are favored as the cell of origin for prostate cancer. Cell Rep 2014;8:1339–46.
24. Zhou Z, Flesken-Nikitin A, Corney DC, Wang W, Goodrich DW, Roy-Burman P, et al. Synergy of p53 and Rb deficiency in a conditional mouse model for metastatic prostate cancer. Cancer Res 2006; 66:7889–98.
25. Couto SS, Cao M, Duarte PC, Banach-Petrosky W, Wang S, Romanienko P, et al. Simultaneous haploinsufficiency of Pten and Trp53 tumor suppressor genes accelerates tumorigenesis in a mouse model of prostate cancer. Differentiation 2009;77:103–11.
26. Floc'h N, Kinkade CW, Kobayashi T, Aytes A, Lefebvre C, Mitrofanova A, et al. Dual targeting of the Akt/mTOR signaling pathway inhibits castration-resistant prostate cancer in a genetically engineered mouse model. Cancer Res 2012;72:4483–93.
27. Aytes A, Mitrofanova A, Lefebvre C, Alvarez MJ, Castillo-Martin M, Zheng T, et al. Cross-species regulatory network analysis identifies a synergistic interaction between FOXM1 and CENPF that drives prostate cancer malignancy. Cancer Cell 2014;25:638–51.
28. Best CJ, Gillespie JW, Yi Y, Chandramouli GV, Perlmutter MA, Gathright Y, et al. Molecular alterations in primary prostate cancer after androgen ablation therapy. Clin Cancer Res 2005;11:6823–34.
29. Li Z, Alyamani M, Li J, Rogacki K, Abazeed M, Upadhyay SK, et al. Redirecting abiraterone metabolism to fine-tune prostate cancer antiandrogen therapy. Nature 2016;533:547–51.
30. Li Z, Bishop AC, Alyamani M, Garcia JA, Dreicer R, Bunch D, et al. Conversion of abiraterone to D4A drives anti-tumour activity in prostate cancer. Nature 2015;523:347–51.
31. Mostaghel EA, Marck BT, Plymate SR, Vessella RL, Balk S, Matsumoto AM, et al. Resistance to CYP17A1 inhibition with abiraterone in castration-resistant prostate cancer: induction of steroidogenesis and androgen receptor splice variants. Clin Cancer Res 2011;17:5913–25.
32. Hill R, Song Y, Cardiff RD, Van Dyke T. Selective evolution of stromal mesenchyme with p53 loss in response to epithelial tumorigenesis. Cell 2005;123:1001–11.
33. Mitrofanova A, Aytes A, Zou M, Shen MM, Abate-Shen C, Califano A. Predicting drug response in human prostate cancer from preclinical analysis of in vivo mouse models. Cell Rep 2015;12:2060–71.
34. Stanbrough M, Bubley GJ, Ross K, Golub TR, Rubin MA, Penning TM, et al. Increased expression of genes converting adrenal androgens to testosterone in androgen-independent prostate cancer. Cancer Res 2006;66:2815–25.
35. Sboner A, Demichelis F, Calza S, Pawitan Y, Setlur SR, Hoshida Y, et al. Molecular sampling of prostate cancer: a dilemma for predicting disease progression. BMC Med Genomics 2010;3:8.
36. Bergsland M, Werme M, Malewicz M, Perlmann T, Muhr J. The establishment of neuronal properties is controlled by Sox4 and Sox11. Genes Dev 2006;20:3475–86.
37. Bhattaram P, Penzo-Mendez A, Sock E, Colmenares C, Kaneko KJ, Vassilev A, et al. Organogenesis relies on SoxC transcription factors for the survival of neural and mesenchymal progenitors. Nat Commun 2010;1:9.
38. Sock E, Rettig SD, Enderich J, Bosl MR, Tamm ER, Wegner M. Gene targeting reveals a widespread role for the high-mobility-group transcription factor Sox11 in tissue remodeling. Mol Cell Biol 2004;24: 6635–44.
39. Akdemir KC, Jain AK, Allton K, Aronow B, Xu X, Cooney AJ, et al. Genome-wide profiling reveals stimulus-specific functions of p53 during differentiation and DNA damage of human embryonic stem cells. Nucleic Acids Res 2014;42:205–23.
40. Kela I, Harmelin A, Waks T, Orr-Urtreger A, Domany E, Eshhar Z. Interspecies comparison of prostate cancer gene-expression profiles reveals genes associated with aggressive tumors. Prostate 2009;69:1034–44.
41. Berruti A, Mosca A, Porpiglia F, Bollito E, Tucci M, Vana F, et al. Chromogranin A expression in patients with hormone naive prostate cancer predicts the development of hormone refractory disease. J Urol 2007;178:838–43.
42. Hirano D, Okada Y, Minei S, Takimoto Y, Nemoto N. Neuroendocrine differentiation in hormone refractory prostate cancer following androgen deprivation therapy. Eur Urol 2004;45:586–92.
43. Utikal J, Polo JM, Stadtfeld M, Maherali N, Kulalert W, Walsh RM, et al. Immortalization eliminates a roadblock during cellular reprogramming into iPS cells. Nature 2009;460:1145–8.
44. Marion RM, Strati K, Li H, Murga M, Blanco R, Ortega S, et al. A p53-mediated DNA damage response limits reprogramming to ensure iPS cell genomic integrity. Nature 2009;460:1149–53.
45. Kawamura T, Suzuki J, Wang YV, Menendez S, Morera LB, Raya A, et al. Linking the p53 tumour suppressor pathway to somatic cell reprogramming. Nature 2009;460:1140–4.
46. Rasmussen MA, Holst B, Tumer Z, Johnsen MG, Zhou S, Stummann TC, et al. Transient p53 suppression increases reprogramming of human fibroblasts without affecting apoptosis and DNA damage. Stem Cell Rep 2014;3:404–13.
47. Yi L, Lu C, Hu W, Sun Y, Levine AJ. Multiple roles of p53-related pathways in somatic cell reprogramming and stem cell differentiation. Cancer Res 2012;72:5635–45.
48. Greenberg NM, DeMayo F, Finegold MJ, Medina D, Tilley WD, Aspinall JO, et al. Prostate cancer in a transgenic mouse. Proc Natl Acad Sci U S A 1995;92:3439–43.
49. Masumori N, Thomas TZ, Chaurand P, Case T, Paul M, Kasper S, et al. A probasin-large T antigen transgenic mouse line develops prostate adenocarcinoma and neuroendocrine carcinoma with metastatic potential. Cancer Res 2001;61:2239–49.
50. Ku SY, Rosario S, Wang Y, Mu P, Seshadri M, Goodrich ZW, et al. Rb1 and Trp53 cooperate to suppress prostate cancer lineage plasticity, metastasis, and antiandrogen resistance. Science 2017;355:78–83.
51. Mu P, Zhang Z, Benelli M, Karthaus WR, Hoover E, Chen CC, et al. SOX2 promotes lineage plasticity and antiandrogen resistance in TP53- and RB1-deficient prostate cancer. Science 2017;355:84–8.
52. Ferone G, Song JY, Sutherland KD, Bhaskaran R, Monkhorst K, Lambooij JP, et al. SOX2 Is the determining oncogenic switch in promoting lung squamous cell carcinoma from different cells of origin. Cancer Cell 2016;30:519–32.
53. Bergsland M, Ramskold D, Zaouter C, Klum S, Sandberg R, Muhr J. Sequentially acting Sox transcription factors in neural lineage development. Genes Dev 2011;25:2453–64.
54. Bishop JL, Thaper D, Vahid S, Davies A, Ketola K, Kuruma H, et al. The master neural transcription factor BRN2 is an androgen receptor-suppressed driver of neuroendocrine differentiation in prostate cancer. Cancer Discov 2017;7:54–71.
55. Dardenne E, Beltran H, Benelli M, Gayvert K, Berger A, Puca L, et al. N-Myc induces an EZH2-mediated transcriptional program driving neuroendocrine prostate cancer. Cancer Cell 2016;30:563–77.
56. Lee JK, Phillips JW, Smith BA, Park JW, Stoyanova T, McCaffrey EF, et al. N-Myc drives neuroendocrine prostate cancer initiated from human prostate epithelial cells. Cancer Cell 2016;29:536–47.
57. Hubbard GK, Mutton LN, Khalili M, McMullin RP, Hicks JL, Bianchi-Frias D, et al. Combined MYC activation and pten loss are sufficient to create genomic instability and lethal metastatic prostate cancer. Cancer Res 2016;76:283–92.
58. Kretzschmar K, Watt FM. Lineage tracing. Cell 2012;148:33–45.
59. Lotan TL, Gupta NS, Wang W, Toubaji A, Haffner MC, Chaux A, et al. ERG gene rearrangements are common in prostatic small cell carcinomas. Mod Pathol 2011;24:820.
60. Sequist LV, Waltman BA, Dias-Santagata D, Digumarthy S, Turke AB, Fidias P, et al. Genotypic and histological evolution of lung cancers acquiring resistance to EGFR inhibitors. Sci Transl Med 2011;3:75ra26.
61. Niederst MJ, Sequist LV, Poirier JT, Mermel CH, Lockerman EL, Garcia AR, et al. RB loss in resistant EGFR mutant lung adenocarcinomas that transform to small-cell lung cancer. Nat Commun 2015;6:6377.